Interactive CardioVascular and Thoracic Surgery 24 (2017) 82–89
doi:10.1093/icvts/ivw296 Advance Access publication 13 September 2016

ORIGINAL ARTICLE

Cite this article as: Tanaka A, Kawaji K, Patel AR, Ota T. The extracellular matrix patch implanted in the right ventricle evaluated with cardiovascular magnetic resonance protocol to assess regional physio-mechanical properties. Interact CardioVasc Thorac Surg 2017;24:82–9.

The extracellular matrix patch implanted in the right ventricle evaluated with cardiovascular magnetic resonance protocol to assess regional physio-mechanical properties

Akiko Tanaka[a], Keigo Kawaji[b], Amit R. Patel[b] and Takeyoshi Ota[a,*]

[a] Section of Cardiac and Thoracic Surgery, Department of Surgery, The University of Chicago, Chicago, IL, USA
[b] Section of Cardiology, Department of Medicine, The University of Chicago, Chicago, IL, USA

* Corresponding author. Department of Surgery, Section of Cardiac and Thoracic Surgery, The University of Chicago, 5841 S Maryland Avenue, MC5040, Chicago, IL 60637, USA. Tel: +1-773-7022500; fax: +1-773-8349114; e-mail: tota@surgery.bsd.uchicago.edu (T. Ota).

Received 2 February 2016; received in revised form 23 June 2016; accepted 25 July 2016

Abstract

OBJECTIVES: An extracellular matrix patch was implanted in the porcine right ventricle for *in situ* myocardial regeneration. A newly developed cardiovascular magnetic resonance protocol was utilized to investigate the regional physio-mechanical function of the patch.

METHODS: Cardiovascular magnetic resonance was performed at 60-day after the porcine right ventricular wall full thickness substitution with an extracellular matrix cardiac patch ($n = 5$). Dacron patches and remote normal right ventricle served as control ($n = 5$/each). Late gadolinium enhancement, strain encoding and rest perfusion were measured for scar/patch detection, regional contractility and tissue perfusion. Image analyses were performed by two observers to validate interobserver reproducibility.

RESULTS: All imaging sequences were successfully obtained. The patches were located with late gadolinium enhancement imaging in 95% accuracy. All the parameters demonstrated significant differences among extracellular matrix, Dacron and normal myocardium ($P < 0.05$), which correlated with histological findings, including constructive remodelling with nascent myocardium and profound vasculogenesis/angiogenesis in extracellular matrix patches, and scar formation in Dacron. Bland–Altman analysis demonstrated good interobserver reproducibility with minimal bias (strain encoding/peak strain: mean difference = −0.32%, 95% limits of agreement = −1.2 to 0.57, correlation = 0.97; rest perfusion/relative maximum upslope: mean difference = −0.74, 95% limits of agreement = −2.0 to 0.53, correlation = 0.92), along with excellent correlation obtained from linear regression (strain encoding: $R^2 = 0.93$; rest perfusion: $R^2 = 0.85$).

CONCLUSIONS: With the cardiovascular magnetic resonance protocol, we successfully confirmed early signs of functional myocardial regeneration in implanted extracellular matrix patches. This approach is promising in assessing *in situ* regional physio-mechanical properties and degree of regeneration of implanted tissue-engineered materials.

Keywords: Cardiovascular magnetic resonance • Right ventricle • Regional mechanical function • Tissue engineering

INTRODUCTION

Tissue-engineered materials have been adapted to treat damaged cardiac tissue and congenital anomalies [1, 2]. An example of such materials is the extracellular matrix derived from the porcine small intestine submucosa (SIS-ECM), which has become commercially available, and its clinical application has expanded in the past decade in the field of cardiac surgery. The implanted SIS-ECM serves as a scaffold which allows site-specific host cell repopulation and subsequent constructive remodelling. However, the detailed *in situ* myocardial regeneration process has not been well described. The conventional methods to evaluate tissue regeneration depend upon post-sacrifice *in vitro* analyses, such as histology and reverse-transcript polymerase chain reaction [3–5]. Only a handful of relevant studies to assess *in vivo* physio-mechanical functions of tissue-engineered material implanted in the heart are available.

Cardiovascular magnetic resonance (CMR) has been widely used to assess the morphology and function of the heart in both clinical and research studies. Recent improvements in hardware and image reconstruction techniques enabled measuring of regional contractility [6] as well as tissue perfusion [7]. However, it is still challenging to assess detailed investigation of regional physio-mechanical properties as well as tissue characterization, especially in the right ventricle.

We have established a CMR protocol to assess detailed physio-mechanical functions in a localized area in the right ventricle. The objective of the present study is to evaluate the feasibility of our CMR protocol to assess the regional physio-mechanical properties of the implanted SIS-ECM patch in a porcine right ventricle model.

METHODS

The position of implanted patches located with the CMR was evaluated against a macro-finding to evaluate the accuracy of detection. The measurements of the patch region from strain and perfusion images were compared against measurements made in the remote normal right ventricular myocardial free wall. The reliability of the protocol was assessed with intra- and interobserver reproducibility. In addition, all these CMR findings were compared with the histological findings of the extracted tissues.

Cardiac patch preparation

SIS-ECM (CorMatrix® Cardiovascular Inc., Roswell, GA, USA) was prepared for surgical implantation by soaking it in 0.9% natural saline (Baxter International Inc., Deerfield, IL, USA) for 30 min at room temperature. For control, a sterilized Dacron patch was implanted for the cardiac repair (Edwards Lifescience Co., Irvine, CA, USA).

Myocardial repair in a porcine model

The study protocol was approved by the Institutional Animal Care and Use Committee of the University of Chicago. All animals received humane care in compliance with the Guide for the Care and Use of Laboratory Animals, published by the National Institutes of Health (1996).

The animals (female, mixed breed of Yorkshire and Landrace, 20–30 kg; $n = 10$) were anaesthetized and placed in a left recumbent position. The heart was exposed via a right anterolateral thoracotomy in the fourth intercostal space. After a bolus of lidocaine (2 mg/kg), a tangential clamp was placed on the right ventricular free wall. The ventricular wall was incised in full thickness and was substituted with a patch (30 mm in diameter) with a 5-0 continuous polypropylene suture (Fig. 1). Routine chest closure was performed. SIS-ECM patches were implanted in five pigs. Similarly, Dacron patches were implanted in five pigs to serve as a control. At 60 days after implantation, the animals were subjected to CMR and were euthanized for further tissue examination.

Cardiovascular magnetic resonance imaging

CMR assessment was performed after the 60-day period to evaluate the regional physio-mechanical properties of the implanted patches and the normal myocardium. All animals were imaged on 1.5 T MRI hardware (Philips Achieva, Best, Netherlands), using a five-channel cardiac array.

Cardiovascular magnetic resonance acquisition. In this protocol, an initial localization scout was examined to determine the approximate right ventricular patch location, using the right anterolateral surgical incision as reference. Next, a two-chamber, four-chamber and short-axis cine-CMR sequences were acquired to plan the following CMR sequences in the short-axis view that covered the right ventricular region containing the patch: (i) strain encoding [6], (ii) first-pass myocardial perfusion [7] and (iii) late gadolinium enhancement. All imaging techniques were performed under respirator-controlled breath holding. For all scans, standard CMR parameters were used: FOV = 300–340 × 300–340 mm^2; slice thickness = 6–10 mm. Additional CMR parameters, including the pulse sequence flip angles, acquisition scheme and window sizes, and repetition/echo time values were all set to their respective default values provided on the scanner hardware. For the strain-encoding sequence, full right ventricle coverage (five to six short-axis slices covering the entire right ventricle) was acquired sequentially, in which all slices were acquired per single breath-hold. To account for the high heart rates, the acquisition was set over 2 (∼1200–1500 ms) electrocardiogram-gated intervals. Contrast injection was performed, using 0.05 mmol/kg of Gadobenate Dimeglumine (Multihance; Bracco Diagnostic Inc., Princeton, NJ, USA) during first-pass perfusion which was imaged, using a hybrid gradient echo/echo-planar imaging sequence (voxel size ∼2.5 × 2.5 mm, slice thickness 10 mm, flip angle 20°, repetition time 5.9 ms, echo time 2.5 ms, echo-planar imaging factor 5, delay time 80 ms and sensitivity encoding factor 1.3) to acquire six SA slices of the identified right ventricle region over every 2R-R (∼1200–1500 ms) electrocardiogram-gated intervals for 50 consecutive heartbeats. Late gadolinium enhancement images were acquired in the short-axis plane 12 min post-contrast (total 0.2 mmol/kg), using a T_1-weighted gradient echo pulse sequence with a phase-sensitive inversion recovery reconstruction (TR 4.5 ms, TE 2.2 ms, TI 250–300 ms, flip angle 30°, flip angle 5°, voxel size 2 × 2 × 10 mm, sensitivity encoding factor 2). Optimal inversion time was chosen based on a TI scout (typically 250–300 ms).

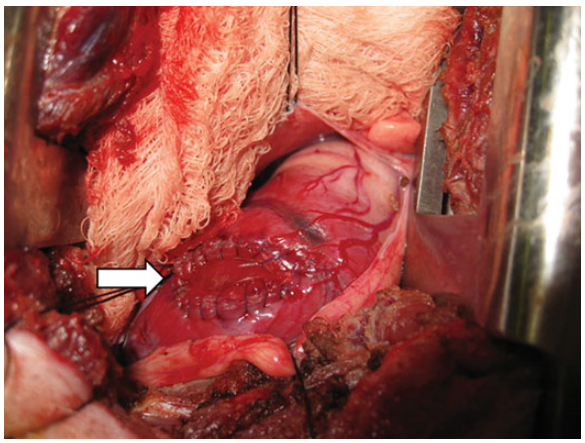

Figure 1: A representative intraoperative surgeon's view of implanted right ventricle patch. White arrow: patch area.

Macro inspection

After the CMR, the pigs were sacrificed. Their excised hearts were first examined for patch position on the right ventricular free wall. The right ventricular free wall was incised at the level of the tricuspid valve and the posterior wall where the interventricular septum attaches. The photograph of the opened free wall was taken to record the patch position (Fig. 2). Then, the patch area was processed for histological analysis.

Cardiovascular magnetic resonance analysis

CMR image analysis was performed by two investigators (observer 1, A.T.; observer 2, T.O.).

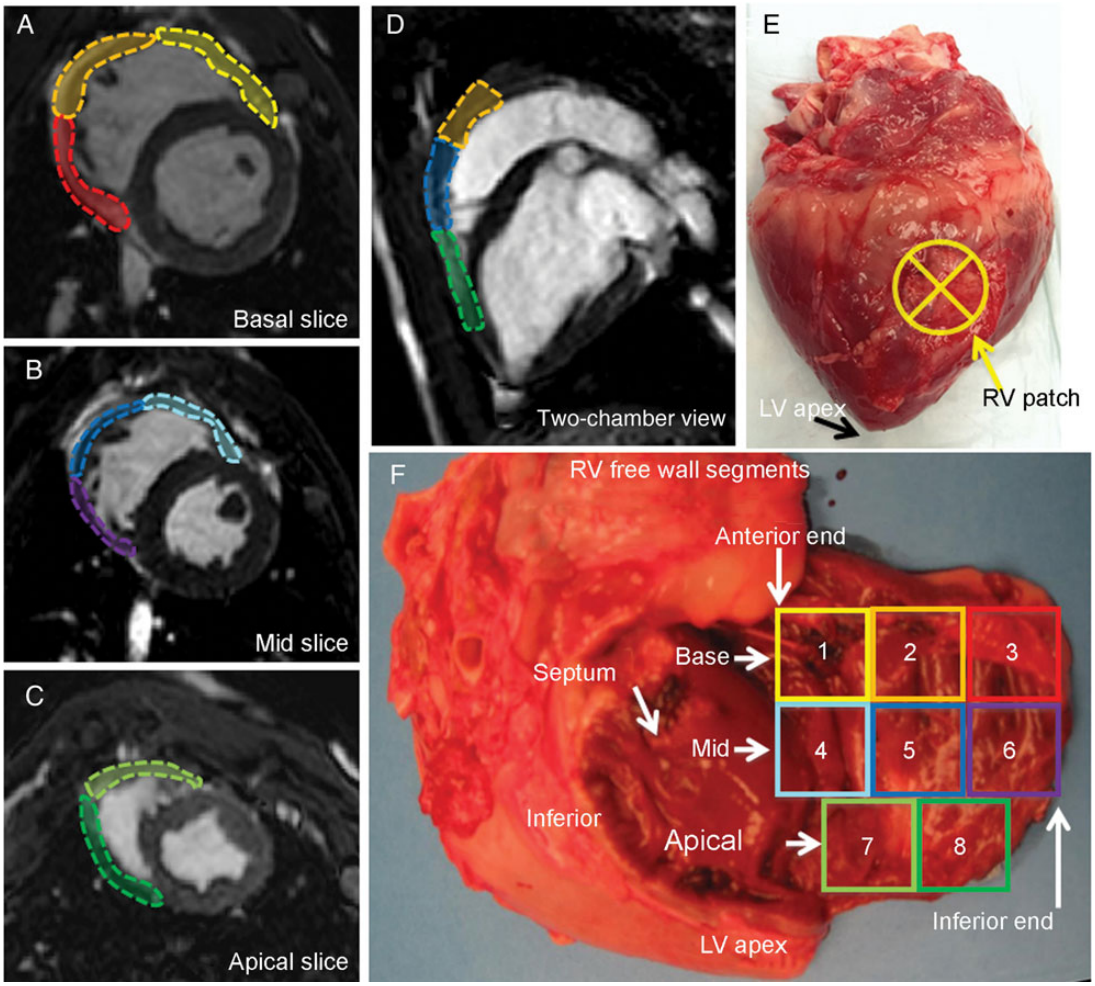

Figure 2: The right ventricular free wall segments. The right ventricular free wall was divided into eight sections using left ventricle segmentation as a reference: (**A**) The basal segment and (**B**) mid segment are further divided into anterior, lateral and inferior segments. (**C**) The apical slice is smaller compared with other two longitudinal segments and is divided into anterior and inferior segments. (**E**) An example of macro inspection of the right ventricle patch on the mid-lateral segment. (**F**) A photograph of the extracted heart with the right ventricle free wall cut at the basal-inferior-apical end and opened. The colour of the eight segments corresponds to A–D. In this specimen, the patch is located in 5, 7 and 8 (i.e. mid apical–lateral wall). Inferior: right ventricular inferior wall; LV: left ventricle; RV: right ventricle; septum: interventricular septum.

Accuracy of scar/patch detection using late gadolinium enhancement. Location of the implanted patch was recorded at the time of sacrifice. The right ventricular free wall was divided into eight sections using left ventricle segmentation [8] as a reference (Fig. 2) to compare the macro data and the patch area located by the 2D-late gadolinium enhancement images (Fig. 3A). All subsequent analysis was performed using the identified patch region (Fig. 3B and C).

Strain encoding. The peak longitudinal strain and time to peak longitudinal strain were analysed using commercial software (Diagnosoft VIRTUE, Diagnosoft, Inc., Morrisville, NC, USA) to determine regional contractility. Regional longitudinal myocardial strain was calculated using a region-of-interest analysis that accounted for local motion through the cardiac cycle [9]. The maximal systolic strain was manually chosen from the time frame that exhibited peak deformation at end-systole (Fig. 3D). The measurement of the strain was performed twice per animal by each observer with minimum 7 days between the initial and subsequent measurements. For the intraobserver variability, the two measurements obtained from observer 1 (A.T.) were analysed. For the interobserver variability, the average values of both observers were examined for interobserver reproducibility.

Rest perfusion. Signal intensity curve analysis was performed on standard clinical workstation (Philips Healthcare, Best, Netherlands). The maximum upslope of contrast enhancement was obtained from signal intensity time course of the patch region of interest and was normalized to the maximum upslope of a region of interest placed in the left ventricular cavity to evaluate the regional microvascular tissue perfusion [10] (Fig. 3E). The measurement of the maximum upslope was performed twice per animal by each observer, with minimum 7 days between the initial and subsequent measurements. For the intraobserver variability, the two measurements obtained from observer 1 (A.T.) were analysed. For the interobserver variability, the average values of both observers were examined for interobserver reproducibility.

Histology and immunohistochemistry

Excised tissues were fixed in 10% formalin for paraffin processing and cut into 5-μm sections. The paraffin sections were

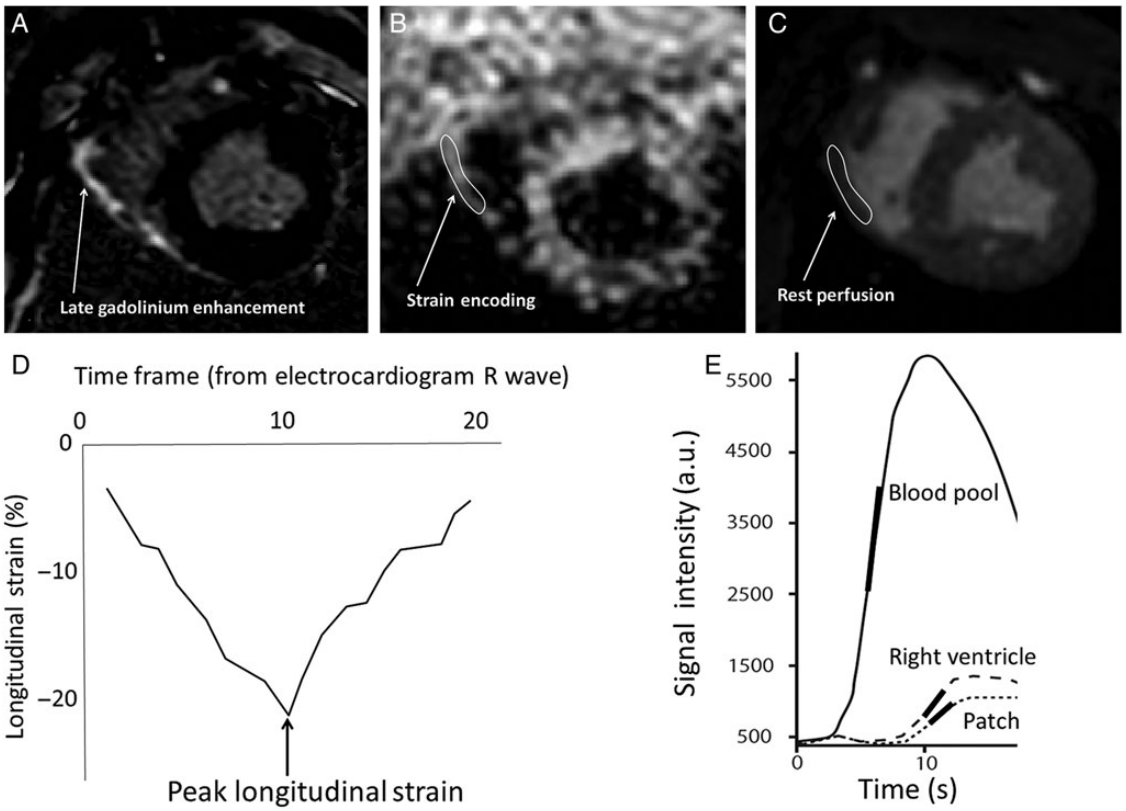

Figure 3: Scheme of analysis for strain encoding and rest perfusion. (**A**) The 2D-late gadolinium enhancement image is used to detect the target lesion along with the macro inspection. Corresponding image slice is selected for (**B**) strain encoding and (**C**) rest perfusion. The region of interest is manually picked which will generate (**D**) longitudinal strain curve and (**E**) signal intensity curve. The arrow and encircled area indicate the location of implanted patch. The peak strain is the value obtained at end-systole (2D). The relative maximum upslope is obtained from the ratio of maximum upslope of the target lesion to the maximum upslope of the blood pool (left ventricular cavity).

deparaffinized and stained with haematoxylin–eosin and Masson's trichrome or prepared for immunohistochemical staining. Monoclonal antibodies specific for factor-VIII-related antigen (Dako, Carpinteria, CA, USA) and a-sarcomeric actinin (Sigma, St Louis, MO, USA) were used. Images for the sections were captured with a microscopic system (DP72, 12.8 MP, Olympus America Inc., Center Valley, PA, USA). Capillary density (number of vessels per millimetre square) was obtained by counting the factor-VIII-related antigen-positive capillaries under the ×200 microscopy [11]. Twenty fields were randomly selected in each patch.

Statistical analysis

All values are expressed as the mean ± standard deviation. The statistical differences in all data were determined by the Fisher's exact *t*-test, the Mann–Whitney test and/or ANOVA. Intra- and interobserver variabilities were calculated from the linear regression analysis. Intra- and interobserver limits of agreements and bias were evaluated using Bland–Altman analysis [12].

RESULTS

Cardiovascular magnetic resonance findings

Imaging was successfully performed on all 10 pigs 60 days after each pig's surgical patch implantation.

Scar/patch detection accuracy with 2D-late gadolinium enhancement. The location of the implanted patch was accurately detected in 10 of 10 studies by observer 1 (A.T.) and 9 of 10 by observer 2 (T.O.) from the 2D-late gadolinium enhancement. The surgical reference indicated patch location in the mid-lateral ($n = 3$, observer 1 = 100%, observer 2 = 100%), mid-lateral inferior ($n = 1$, observer 1 = 100%, observer 2 = 0%), mid apical-lateral ($n = 3$, observer 1 = 100%, observer 2 = 100%), apical-anterior ($n = 2$, observer 1 = 100%, observer 2 = 100%) and apical-anterior posterior ($n = 1$, observer 1 = 100%, observer 2 = 100%) walls.

Strain analysis for regional contractility. Peak longitudinal strain (%) in the area of the patch was significantly greater in SIS-ECM patch compared with that in Dacron patch, whereas SIS-ECM patch was significantly less than the normal myocardium (Fig. 4A): SIS-ECM = −16.1 ± 3.0%, Dacron = −8.9 ± 1.6% and self-controlled normal ventricle = −25.8 ± 2.0%. (SIS-ECM versus Dacron, $P < 0.0001$; SIS-ECM versus normal, $P < 0.0001$; Dacron versus normal, $P < 0.0001$). Linear regression of peak longitudinal strain demonstrated good intra- and interobserver correlation with $R^2 = 0.89$ and 0.93, respectively. Bland–Altman plot of the obtained peak longitudinal strain showed good intraobserver reproducibility with a minimal bias (95% limits of agreement = −1.38 to 0.9, correlation = 0.94 $P = 0.63$) (Fig. 4B), and interobserver bias was −0.32% (95% limits of agreement = −1.20 to 0.57, correlation = 0.97, $P = 0.44$) (Fig. 4C).

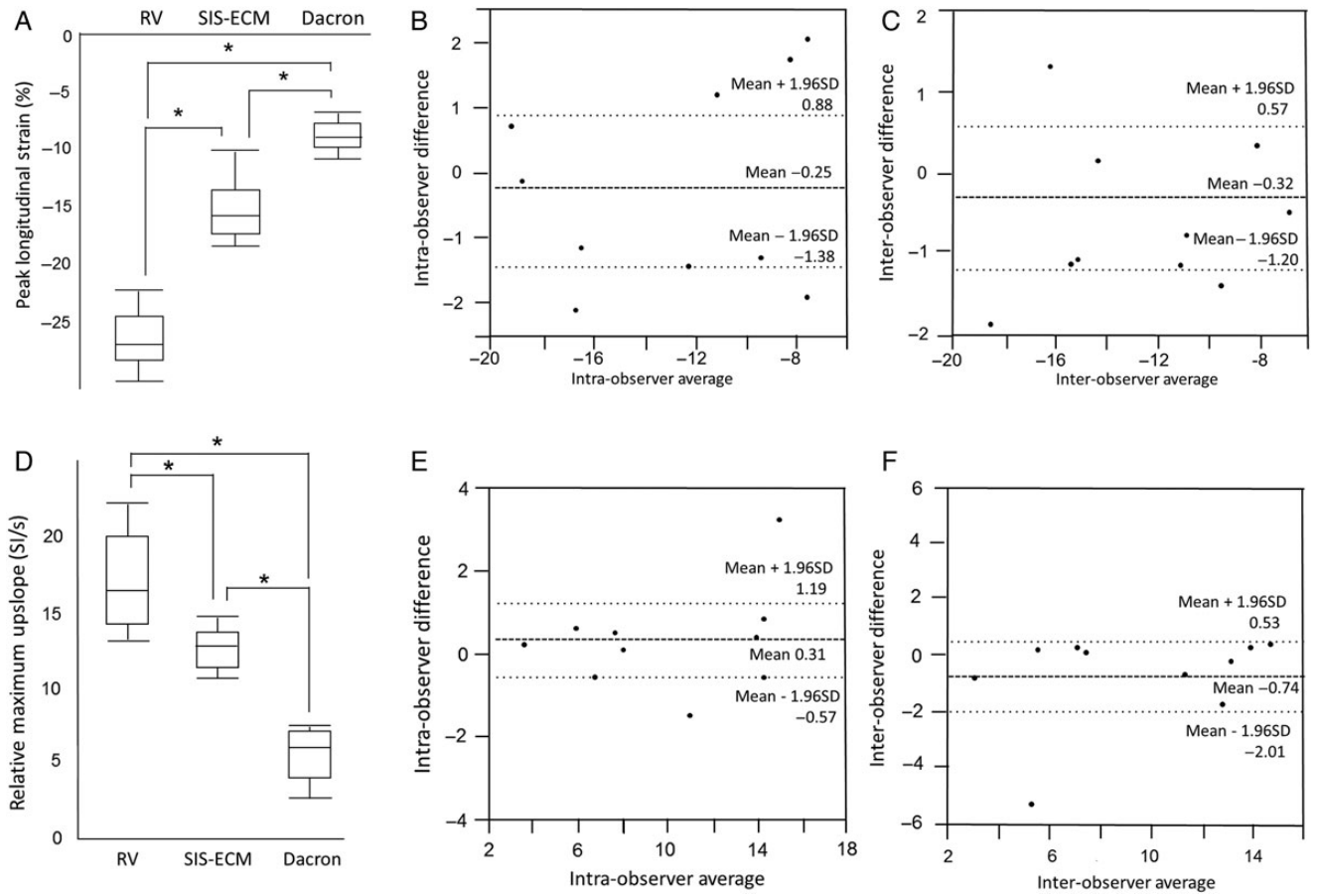

Figure 4: Results of strain encoding and rest perfusion. (**A**) Peak longitudinal strain (strain encoding) and (**D**) relative maximum upslope (rest perfusion) of normal RV, SIS-ECM and Dacron patch is demonstrated. Bland–Altman plot for intraobserver for strain encoding (shown in **B**) and rest perfusion (shown in **E**), and interobserver for strain encoding (shown in **C**) and rest perfusion (shown in **F**) are shown. RV: right ventricle; SIS-ECM: extracellular matrix patch derived from small intestine submucosa.

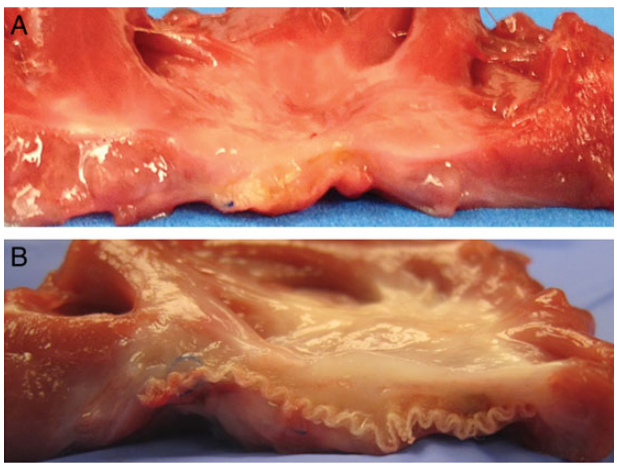

Figure 5: Macro inspection. Cross-section (endocardial surface facing up) of the extracted patch and surrounding at 60 days after implantation. (**A**) Extracellular matrix patch derived from small intestine submucosa; (**B**) Dacron patch.

Relative maximum upslope for regional tissue perfusion. Relative maximum upslope was significantly higher in SIS-ECM patch (13.3 ± 1.3) than in Dacron patch (5.8 ± 2.1) (Fig. 4D). The upslope in normal right ventricular myocardium—16.9 ± 3.0 SI/s—was significantly greater than that of the SIS-ECM patch and Dacron patch ($P < 0.05$). Linear regression analysis of relative maximum upslope demonstrated excellent correlation for intraobserver ($R^2 = 0.92$) and interobserver ($R^2 = 0.85$). Bland–Altman plots for obtained relative maximum upslope demonstrated good intra- and interobserver reproducibilities with biases of 0.31 (95% limits of agreement = −0.57 to 1.20, correlation = 0.96, $P = 0.45$) and −0.74 (95% limits of agreement = −2.0 to 0.53, correlation = 0.92, $P = 0.22$), respectively (Fig. 4E and F).

Macro inspections

The endocardial surface of the SIS-ECM patch was covered with a well-organized thin white layer, and layered tissues on the patch whose thickness were almost equal to that of the normal right ventricular wall (Fig. 5A). A stiff and thick fibrous encapsulation was present on the endocardial side on the Dacron patch (Fig. 5B).

Histology and immunohistochemistry

Histology results are presented in Fig. 6. The histology of SIS-ECM demonstrated that organized cell repopulation was observed around the scaffold collagens that extended towards the endocardial surface. On the other hand, Dacron patch was surrounded by fibrous tissues and inflammatory cells. The cells observed in

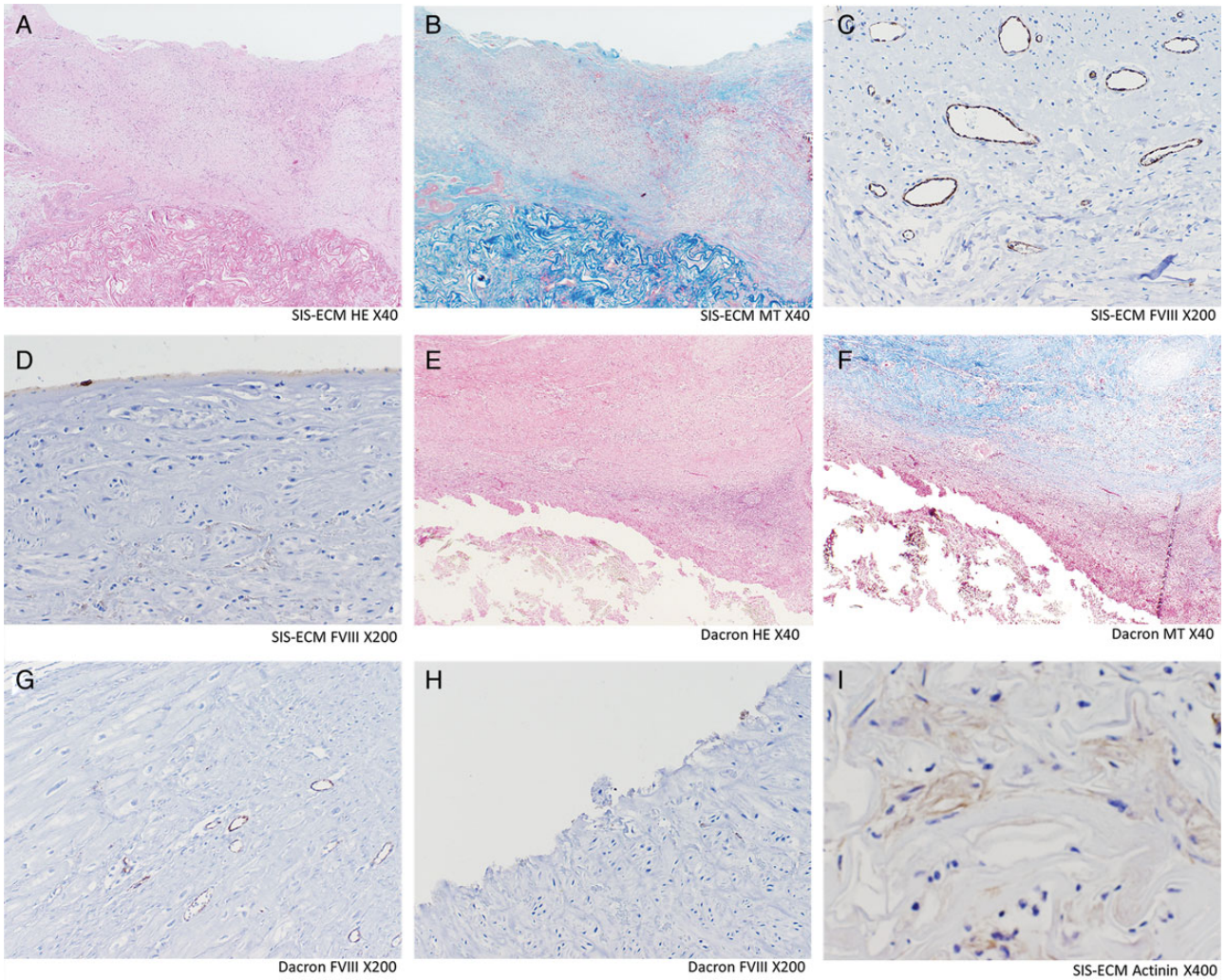

Figure 6: Histology and immunohistochemistry. SIS-ECM (**A**–**D** and **I**): Well-organized cells (shown in A and B) including monolayer of endothelial cells on the endocardial surface (shown in D) and layers of scattered α-sarcomeric actinin-positive cells (shown in I), were observed. The repopulated cells were predominantly observed on the SIS-ECM and extended towards the endocardial surface. Dacron (**E**–**H**): Significant infiltration of lymphoid cells and fibrosis is observed (shown in E and F). No endothelial cells were observed in the endocardial surface (shown in G). Capillary density (C and G): The factor-VIII-related antigen-positive capillaries were counted under the ×200 microscopy for capillary density analysis. Vasculogenesis/angiogenesis was significantly more prevalent in SIS-ECM patch. Dacron: Dacron patch; FVIII: immunohistochemistry staining for factor-VIII-related antigen; HE: haematoxylin–eosin staining; MT: Masson trichrome staining; SIS-ECM: extracellular matrix patch derived from small intestine submucosa.

SIS-ECM were positive for α-sarcomeric actinin, suggesting the presence of nascent cardiomyocytes, whereas that was negative in the Dacron patch. The surface of the SIS-ECM patch was covered with a well-organized monolayer of endothelial cells, but no endothelial cells were found on the Dacron patch. The capillary structures were predominantly distributed in the layers close to the patch materials in the groups of both patches. Vasculogenesis/angiogenesis was assessed by the capillary density, which was significantly greater in the SIS-ECM patch than in the Dacron patch (SIS-ECM 20.9 ± 1.5/mm^2 vs Dacron 7.5 ± 1.3/mm^2, $P < 0.0001$).

DISCUSSION

In the present study, our CMR protocol successfully demonstrated the capability of detecting the small patch areas in the right ventricular free wall. CMR was also able to distinguish among SIS-ECM, Dacron and normal myocardial tissue. The CMR parameters from both SIS-ECM and Dacron patches correlated well with the histological findings. Strain encoding for strain analysis showed positive contractility in the SIS-ECM patch greater than that in the Dacron patch, whereas those were less than the contractility of the normal RV myocardium. It would suggest that the SIS-ECM was in the early phase of functional remodeling, which was supported by the presence of nascent cardiomyocytes (positive alpha-sarcomeric actinin cells) in the histological [13]. The Dacron patch showed little regional contractility and scar tissue formation around the patch consistent with foreign body reaction. First-pass rest perfusion evaluation demonstrated that the tissue perfusion in SIS-ECM was significantly greater than in the Dacron patch. This finding was supported by the result of the capillary density. Intra- and interobserver reliabilities demonstrated good correlation and agreement between repeated measurements with acceptable differences. Thus, the results demonstrate that our CMR protocol was reliable and reproducible.

It is important to note that SIS-ECM patches in this study demonstrated a great potential for reconstructive myocardial

regeneration. While the animals were sacrificed in a relatively short study period (i.e. 60 days after implantation), the implanted SIS-ECM patches already showed significantly repopulated host cells including scattered α-sarcomeric actinin-positive maturing cardiomyocytes. The clinical use of SIS-ECM has increased, and it has been implanted to over 95 000 cardiac procedures. Unlike inert materials (i.e. Dacron), which induce inflammation, calcification and subsequent stiffness over a period of time, SIS-ECM has a predominant potential for cellular repopulation with restoration of regional tissue functionality as well as 'growing' potential [14].

On the other hand, tissue characterization of the remodelled SIS-ECM has been limited to extracted specimens with histology and RT-PCR to identify cell lines (e.g. cardiomyocyte, endothelial cell and mesenchymal cell) [3, 15]. Other reported methodology used for the assessment of remodelled ECM includes video microscope to observe contracting cells [16], and two-photon excitation fluorescence microscopy to image the voltage and calcium ion [17]. All of these *in vitro* procedures can be performed only after the tissue extraction. Several investigators reported *in vivo* assessments with echocardiography or CMR to evaluate the myocardium repaired with tissue-engineering materials. But they are limited to general morphological inspection and global cardiac function assessment, and are unable to assess localized lesions [4, 18]. Electromechanical mapping can assess regional contractility and electrical conductivity of the implanted ECM patches, but it is an invasive procedure and not suitable for repeated evaluation [18, 19]. Our CMR protocol, which is a non-invasive and repeatable scan, can provide *in vivo* assessment of regional physio-mechanical properties in the RV, including biomechanical function (strain) and tissue characteristics (perfusion). It could help us to understand the reconstructive remodelling process correlated with conventional *in vitro* studies.

This study utilized an RV model as it offers a greater challenge for current imaging techniques (e.g. echocardiography, CMR) commonly performed in the LV. The assessment of regional characteristics of the RV myocardium is not as well studied as in the LV. Visualization of the RV is known to be difficult with echocardiography [20]. In addition, commonly used parameters assess functions of the RV as echocardiography has proved to be not reliable in patients with congenital heart disease [21, 22]. Our new CMR protocol would potentially overcome such limitations. In the current study, the thickness of the normal RV free wall, SIS-ECM and Dacron patch regions was between 3.5 and 7 mm. While such thin structures become sensitive to artefacts, such as partial volume effects and motion artefacts during CMR data acquisition, our protocol was capable of obtaining reliable data for small patch areas implanted in the RV. RV function is crucial for patient management in congenital heart disease, heart failure and pulmonary hypertension [23–25]. In particular, the prevalence of adult congenital heart disease has increased by 50% in the past decade and is still growing [26]. Thus, our CMR protocol might also provide a benefit in managing the patients with diseased RVs in the clinical setting as well as assessing the efficacy of tissue-engineering treatment (e.g. tissue-engineered cardiac patch repair, cell injection) as well as improve the current clinical protocol to assess much more detailed regional functions in the left ventricle in the future.

Limitations

The sample size is relatively small although this is a proof-of-concept study. Also, two observers were trained for a short period of time to perform CMR analysis; however, our results demonstrated that even with minimal training, CMR analysis, using conventional post-processing techniques, was able to obtain reliable data and was feasible in this initial pilot study. In addition, we used juvenile pigs that are presumably in a growth phase and high levels of circulating stem and/or progenitor cells. It may have influenced the positive remodelling of the SIS-ECM patches and enhanced the findings of the present CMR analysis. Finally, since this was a proof-of-concept study, we chose to use the RV model to assess the SIS-ECM patch. It, in turn, provided us a good and challenging opportunity to establish a CMR protocol. It would be important to assess SIS-ECM patch in the left-side heart to see its feasibility and durability as further studies.

CONCLUSIONS

Our CMR protocol successfully provided reliable and reproducible data to detect and distinguish the physio-mechanical properties among SIS-ECM patch, Dacron patch and normal myocardium in the RV. A comprehensive CMR evaluation might be a powerful tool for *in vivo* assessments to evaluate tissue-engineered materials implanted into the heart.

This study was supported by the American Heart Association Scientist Development Grant (PI T.O.; 11SDG5120010), the National Center for Advancing Translational Sciences of the National Institutes of Health (PI T.O.; UL1 TR000430) and Institute of Translational Medicine Pilot Award (PI K.K.; CTSA UL1 TR000430). A.R. P. receives research support from Philips Healthcare.

Conflict of interest: none declared.

REFERENCES

[1] Badylak SF. The extracellular matrix as a biologic scaffold material. Biomaterials 2007;28:3587–93.
[2] Quarti A, Nardone S, Colaneri M, Santoro G, Pozzi M. Preliminary experience in the use of an extracellular matrix to repair congenital heart diseases. Interact CardioVasc Thorac Surg 2011;13:569–72.
[3] Ota T, Gilbert TW, Schwartzman D, McTiernan CF, Kitajima T, Ito Y *et al.* A fusion protein of hepatocyte growth factor enhances reconstruction of myocardium in a cardiac patch derived from porcine urinary bladder matrix. J Thorac Cardiovasc Surg 2008;136:1309–17.
[4] Yanagawa B, Rao V, Yau TM, Cusimano RJ. Potential myocardial regeneration with cormatrix ECM: a case report. J Thorac Cardiovasc Surg 2014; 147:e41–3.
[5] Sekine H, Shimizu T, Hobo K, Sekiya S, Yang J, Yamato M *et al.* Endothelial cell coculture within tissue-engineered cardiomyocyte sheets enhances neovascularization and improves cardiac function of ischemic hearts. Circulation 2008;118(14 Suppl):S145–52.
[6] Osman NF, Sampath S, Atalar E, Prince JL. Imaging longitudinal cardiac strain on short-axis images using strain-encoded MRI. Magn Reson Med 2001;46:324–34.
[7] Wilke NM, Jerosch-Herold M, Zenovich A, Stillman AE. Magnetic resonance first-pass myocardial perfusion imaging: clinical validation and future applications. J Magn Reson Imaging 1999;10:676–85.
[8] Cerqueira MD, Weissman NJ, Dilsizian V, Jacobs AK, Kaul S, Laskey WK *et al.* Standardized myocardial segmentation and nomenclature for tomographic imaging of the heart. A statement for Healthcare Professionals from the Cardiac Imaging Committee of the Council on Clinical Cardiology of the American Heart Association. Circulation 2002;105: 539–42.

[9] Hamdan A, Thouet T, Kelle S, Paetsch I, Gebker R, Wellnhofer E *et al.* Regional right ventricular function and timing of contraction in healthy volunteers evaluated by strain-encoded MRI. J Magn Reson Imaging 2008;28:1379–85.
[10] Schuleri KH, Amado LC, Boyle AJ, Centola M, Saliaris AP, Gutman MR *et al.* Early improvement in cardiac tissue perfusion due to mesenchymal stem cells. Am J Physiol Heart Circ Physiol 2008;294:H2002–11.
[11] Kobayashi T, Hamano K, Li TS, Katoh T, Kobayashi S, Matsuzaki M *et al.* Enhancement of angiogenesis by the implantation of self bone marrow cells in a rat ischemic heart model. J Surg Res 2000;89:189–95.
[12] Bland JM, Altman DG. Statistical methods for assessing agreement between two methods of clinical measurement. Lancet 1986;1:307–10.
[13] Lu MH, DiLullo C, Schultheiss T, Holtzer S, Murray JM, Choi J *et al.* The vinculin/sarcomeric-alpha-actinin/alpha-actin nexus in cultured cardiac myocytes. J Cell Biol 1992;117:1007–22.
[14] Maeda K, Ruel M. The clinical application potential of extracellular matrix in cardiac tissue engineering. J Thorac Cardiovasc Surg 2015;150:1290–1.
[15] Xu Y, Patnaik S, Guo X, Li Z, Lo W, Butler R *et al.* Cardiac differentiation of cardiosphere-derived cells in scaffolds mimicking morphology of the cardiac extracellular matrix. Acta Biomater 2014;10:3449–62.
[16] Narmoneva DA, Vukmirovic R, Davis ME, Kamm RD, Lee RT. Endothelial cells promote cardiac myocyte survival and spatial reorganization: implications for cardiac regeneration. Circulation 2004;110:962–6.
[17] Ghouri IA, Kelly A, Burton FL, Smith GL, Kemi OJ. 2-photon excitation fluorescence microscopy enables deeper high-resolution imaging of voltage and Ca(2+) in intact mice, rat, and rabbit hearts. J Biophotonics 2015;8:112–23.
[18] Miyagi Y, Zeng F, Huang XP, Foltz WD, Wu J, Mihic A *et al.* Surgical ventricular restoration with a cell- and cytokine-seeded biodegradable scaffold. Biomaterials 2010;31:7684–94.
[19] Ota T, Gilbert TW, Badylak SF, Schwartzman D, Zenati MA. Electromechanical characterization of a tissue-engineered myocardial patch derived from extracellular matrix. J Thorac Cardiovasc Surg 2007; 133:979–85.
[20] Sanz J, Conroy J, Narula J. Imaging of the right ventricle. Cardiol Clin 2012; 30:189–203.
[21] Mercer-Rosa L, Parnell A, Forfia PR, Yang W, Goldmuntz E, Kawut SM. Tricuspid annular plane systolic excursion in the assessment of right ventricular function in children and adolescents after repair of tetralogy of Fallot. J Am Soc Echocardiogr 2013;26:1322–9.
[22] Selly JB, Iriart X, Roubertie F, Mauriat P, Marek J, Guilhon E *et al.* Multivariable assessment of the right ventricle by echocardiography in patients with repaired tetralogy of Fallot undergoing pulmonary valve replacement: a comparative study with magnetic resonance imaging. Arch Cardiovasc Dis 2015;108:5–15.
[23] Kohler D, Arnold R, Loukanov T, Gorenflo M. Right ventricular failure and pathobiology in patients with congenital heart disease - implications for long-term follow-up. Front Pediatr 2013;1:37.
[24] Aronson D, Darawsha W, Atamna A, Kaplan M, Makhoul BF, Mutlak D *et al.* Pulmonary hypertension, right ventricular function, and clinical outcome in acute decompensated heart failure. J Card Fail 2013;19: 665–71.
[25] Junqueira FP, Macedo R, Coutinho AC, Loureiro R, De Pontes PV, Domingues RC *et al.* Myocardial delayed enhancement in patients with pulmonary hypertension and right ventricular failure: evaluation by cardiac MRI. Br J Radiol 2009;82:821–6.
[26] Marelli AJ, Ionescu-Ittu R, Mackie AS, Guo L, Dendukuri N, Kaouache M. Lifetime prevalence of congenital heart disease in the general population from 2000 to 2010. Circulation 2014;130:749–56.